

**Bubble Nucleation, Growth and Surface Temperature Oscillations on a Rapidly  
Heated Microscale Surface immersed in a Bulk Subcooled but Locally  
Superheated Liquid under Partial Vacuum**

Richard E. Cavicchi<sup>1</sup> and C. Thomas Avedisian<sup>2,†</sup>

<sup>1</sup>Process Measurements Division

National Institute of Standards and Technology

Gaithersburg, Md. 20899

<sup>2</sup>Sibley School of Mechanical and Aerospace Engineering

Cornell University

Ithaca, New York 14853-7501

---

<sup>†</sup>author of correspondence: cta2@cornell.edu; phone, 607-592-7915; fax, 607-255-1222

## **Abstract**

The effect of ambient pressures below atmospheric, liquid subcooling and heating rate on bubble dynamics associated with rapid evaporation in highly superheated water is investigated. Platinum films of various aspect ratios are electrically heated under partial vacuum and the average metal film temperature monitored during a power pulse of duration of several tens of microseconds.

At high liquid subcooling, the surface temperature of the pulse-heated thin platinum strips is shown to oscillate with a frequency on the order of 0.5 MHz. The oscillation frequency increases with ambient pressure in the range 0.02MPa and 0.101MPa, and decreases with increasing ambient temperature at a fixed pressure. An unusual dynamic instability is observed in which the surface temperature is constant before relaxing into oscillations, and the delay to oscillations increases with decreasing pressure.

High speed imaging shows that the bubble growth phase of the oscillation is associated with surface heating and the collapse phase with surface cooling in the cyclic temperature history. These effects are explained by a bubble growth theory that includes a heat loss mechanism to the surrounding liquid. The nucleation temperature is unaffected by pressure in the sub-atmospheric range examined and it approaches the theoretical superheat limit for water at a heating rate of about  $10^9$  °C/s.

Keywords: boiling, superheated liquid, homogeneous nucleation, bubble nucleation, surface tension, bubble growth, condensation, temperature oscillations

## Introduction

Bubble nucleation and growth on microscale surfaces<sup>1</sup> immersed in sub-cooled liquids is an important process in applications that use bubble formation as a means to push fluid through microscale structures, as in thermal ink jet printing [2,3] and bubble pump designs [4-6]. Many parameters influence the phase change dynamics on microscale surfaces including gravity, liquid subcooling, and heater size [1,7,8] and pressure. Under some conditions the surface temperature can oscillate during the phase change process. Observed in the post-nucleation regime, oscillations have been noted for 65  $\mu\text{m}$  square thin metal films immersed in water and aqueous methanol mixtures [9,10], 100  $\mu\text{m}$  diameter by 4 cm long platinum wires in organic fluids [11] and for sub-microscale surfaces [12] under atmospheric pressure conditions. The existence of oscillations may signal an erratic bubble dynamic that influences the quality of the droplet ejection process and is therefore important to understand.

With reference to figure 1, five periods characterize the overall processes leading up to surface temperature oscillations for a microscale surface with a sustain constant heat input: an initial surface heating profile (1) that consists of a somewhat exponential form associated with liquid heating; a transition period (2) marked by an inflection point in the evolution of average surface temperature that signifies the state where a bubble is nucleated; a period similar to the first (3) but with an initially higher heating rate because heat transfer is now across a vapor layer (with lower thermal conductivity compared to the liquid) because the nucleated bubble expands laterally over the surface; and remaining periods where the surface temperature is constant (4) followed by an oscillatory period (5) that can sustain itself indefinitely for a constant heat input.

The present investigation is undertaken to further examine the surface temperature oscillation phenomenon and conditions that affect it. In particular, the influence of surface heating rate, ambient pressures below atmospheric, and bulk liquid subcooling are considered for heating times on the order of several tens of microseconds. By imposing sub-atmospheric pressure conditions the nucleation temperature will be constant. In saturated or superheated liquids, bubbles should always grow and not collapse and temperature oscillations should not occur. Thin metal films of high aspect ratio (AR) are employed to promote uniform surface temperatures during

---

<sup>1</sup>A microscale surface is one for which the characteristic length of the heater,  $L$ , is much smaller than the Taylor wavelength [1]

$L_{\text{Tay}} = \sqrt{\frac{\sigma}{g(\rho_L - \rho_g)}}$ . For water at 403K (the reference temperature at which properties in Table 1 are evaluated in the present study),  $L_{\text{Tay}} \approx 2$  mm, though heaters with much smaller  $L$  (order of less than 100  $\mu\text{m}$ ) are used in this study.

power pulses so that bulk subcooling will provide the primary mechanism for the collapse process that leads to surface quenching and an oscillating temperature history.

Water is selected as the working fluid because of the extensive property database available for it and familiarity with related experiments of rapid evaporation at the superheat limit [9,10,13-16]. Since surface temperature oscillations are speculated to track with bubble growth and collapse cycles as suggested by the schematics of figures 1b and 1c, some visualizations of bubble morphology are also included using a laser flash method described previously [13]. For these visualizations, ethanol proved to have a slightly more repeatable bubble morphology for the long pulse times investigated compared to water so some results on bubble dynamics are shown for ethanol and correlated to the temperature cycle.

## Experiment

The heaters employed in the present investigation are layered structures consisting of a 300  $\mu\text{m}$  thick Si wafer substrate, a 200 nm thick  $\text{SiO}_2$  insulating layer, a 30-nm-thick titanium adhesion layer and a 200 nm thick Pt film on which the boiling process occurred. Figure 2 is a cross-sectional schematic of the heater structure. Experiments were carried on platinum (Pt) films fabricated into several different ARs to facilitate measurements of the inflection point, delay time and oscillation frequency and photographing bubble shapes by high speed imaging. No single AR could allow for all such information.

Three ARs were examined. A 3  $\mu\text{m}$  x 200  $\mu\text{m}$  (AR=66.7) Pt film was used for measurements of  $T_{\text{nuc}}$  because temperature is uniform along the length of such films. This device is essentially the same as used in a previous study [14]. Figure 3 shows a photomicrograph of a representative heater. High AR films are not suitable for temperature oscillation studies because different boiling modes can co-exist over long surfaces, as shown in some visualizations of explosive bubble growth on 1.91 cm by 3.81 cm gold films in R-113 ( $\text{CCl}_2\text{FCClF}_2$ ) [17]. Reducing the heater area appears to make the bubble morphology slightly more uniform by confining the bubble to a smaller footprint, which also facilitates photographing the bubble during its growth/collapse cycle. A 4  $\mu\text{m}$  x 40  $\mu\text{m}$  (AR=10) Pt film and a 7  $\mu\text{m}$  x 46  $\mu\text{m}$  (AR=6.6) Pt film were used for recording surface temperature oscillations and for photographing bubbles, respectively. Voltage pulses ranged from 30  $\mu\text{s}$  to 90  $\mu\text{s}$  for the detailed observations reported here.

The metal films were heated by passing a current through them. The films formed one leg of a Wheatstone bridge circuit as illustrated in figure 4. The arrangement is similar to that described previously [14]. The bridge consists of the Pt film heater (resistance of  $R_H$ ) in series with a lead resistance  $R_L$  due to the electrical connections. The Si chip with platinum metallization is

glued into a dual-in-line (DIP) package. Gold wire bonds provide electrical connections to the instrumentation. A potentiometer on the opposite leg of the bridge ( $R_3$ ) allows for balancing the bridge. The DIP is placed in a vacuum chamber with electrical connections provided by vacuum feed-throughs. Pressures ranging from 0.02 MPa to 0.101MPa, as measured by a capacitance manometer gauge, were studied. The lower limit was still large enough that water would not immediately evaporate when exposed to a partial vacuum of this level.

Input power was provided by signal generators capable of producing a time dependent input voltage,  $V_{in} = V_o + \gamma t$ , as either a square wave input voltage  $V_{in} = V_o$  ( $\gamma = 0$  by an Agilent 8411 pulse generator), or a linear ramped  $V_{in} = \gamma t$  ( $V_o = 0$  by a Wavetek #143, 20MHz, signal generator). These two forms served several purposes. The ramp input facilitated a gradual surface temperature increase and more precise control of the heating rate at the nucleation temperature. A pulse input allowed for higher heating rates before bubble nucleation, though with less control of the heating rate at the inflection point. The data were stored on a PC interfaced with a digital oscilloscope (LeCroy LT354) through LabView control to record the evolution of  $V_{out}$ .

For a balanced bridge ( $R_1 = R_2$ ,  $R_3 = R_T$ ) input power  $p_{in}$  is related to  $V_{in}$  as

$$p_{in} = V_{in}(t) \frac{R_T}{(R_1 + R_T)^2} \quad 1$$

where  $R_H$  is related to  $R_T$  as  $R_H = R_T - R_L$ . The lithography to fabricate the AR=10 heaters included metal lines that connected to the smaller heater. These lines contributed a significant lead resistance,  $R_L = 21.0 \Omega$ . This correction to  $R_T$  was necessary to convert  $R_H$  to temperature for this film. The metalized pattern for the AR=66.7 film consisted of the long heater directly connected to the wire bond pad, essentially making  $R_L \ll R_T$  for this aspect ratio.

$R_H$  was calibrated by measuring its electrical resistance as a function of temperature in a temperature-controlled furnace. The results are correlated as

$$R_H = R_\infty (1 + \xi(T_H - T_\infty)) \quad 2$$

where  $R_\infty$  is the platinum film resistance at  $T_\infty = 22 \text{ }^\circ\text{C}$  and  $\xi$  is the coefficient of thermal resistance (CTR). For the AR=67.7 film,  $\xi \approx 0.0025 \text{ }^\circ\text{C}^{-1}$  [14] and for the AR=10 film  $\xi \approx 0.0018 \text{ }^\circ\text{C}^{-1}$ . The difference in these CTRs is the result of annealing the AR=66.7 film during fabrication, while no

annealing was done for the AR=10 film. For the AR=66.7 film  $R_1 = R_2 = 38.33\Omega$  was used in the bridge, and  $R_\infty = 51.16 \Omega$ . For the AR=10 film,  $R_1=R_2= 56.0 \Omega$  was used in the bridge and  $R_\infty = 38.0\Omega$ .

Experiments were carried out to show the variation of nucleation temperature with heating rate on the AR = 66.7 films as they provide a more uniform temperature and therefore a more accurate nucleation temperature. The heating rates ranged from  $10^3 \text{ }^\circ\text{C/s}$  to  $10^8 \text{ }^\circ\text{C/s}$  for the ramp input, and from  $10^7 \text{ }^\circ\text{C/s}$  to  $10^9 \text{ }^\circ\text{C/s}$  for the pulse  $V_{in}$ . The form of  $p_{in}(t)$  follows  $V_{in}(t)$  within about 12% over temperatures ranging from 22C to 300C for the AR=66.7 film and within about 8% for the AR=10 film. As such,  $p_{in}(t) \propto V_{in}(t)$ , or  $p_{in} = p_o + \epsilon t$ . Experiments were carried out using deionized high-resistivity 18 M $\Omega$ -cm water, which covered the Pt heater during the voltage pulse. A 500  $\mu\text{L}$  drop of water flooded the surface of each chip during an experiment.

Some limited visualizations of the evolution of bubble morphology were obtained on the AR=6.6 platinum film during a power pulse using a high-speed laser-flash method [13]. This information determines the extent to which growth/collapse cycles qualitatively track with surface temperature oscillations. The ability to obtain this correlation by microphotography that captures one image per pulse is somewhat problematic when the bubble dynamic does not have especially good stability and repeatability at each instant. Water was problematic in this regard for the long power pulses examined in the present study, on the order of tens of microseconds (whereas for short pulses, on the order of a few  $\mu\text{s}$ , bubbles forming in superheated water by rapid evaporation showed good repeatability [15,16]). Bubble formation in superheated ethanol showed much less pulse-to-pulse variations than water though there was still some variability from pulse to pulse for a fixed delay after the start of a pulse. Accordingly, time-lapsed sequences of bubble growth and collapse in ethanol are used to show the extent to which the growth/collapse cycle tracks with surface temperature.

## Results and Discussions

Figure 5 shows representative data for the evolution of average surface temperature for a 2  $\mu\text{s}$  square pulse (5a) and a 275  $\mu\text{s}$  ramped pulse (5b) at 0.101MPa. The input for both pulses was adjusted so that the inflection points signifying nucleation occurred near the end of the pulse. For the pulse input ( $\gamma = 0$ ,  $V_o \neq 0$ , figure 5a) the evolution of average platinum surface temperature is

such that  $\left. \frac{dT}{dt} \right|_{t=0} > 0$  and  $\left. \frac{d^2T}{dt^2} \right|_{t \geq 0} < 0$  while for the ramp input ( $V_o = 0, \gamma \neq 0$ , figure 5b),  $\left. \frac{dT}{dt} \right|_{t=0} = 0$  and  $\left. \frac{d^2T}{dt^2} \right|_{t \geq 0} > 0$ . These trends are explained as follows.

Taking the finite-sized metal film at the interface between two semi-infinite media, assuming that the temperature distribution in each region (solid and liquid) instantaneously adjusts to changes in the film temperature, that the pulse duration is short enough that conduction in the fluid is the only mode of heat transfer, designating “S” as a suitable shape factor for conduction from the film to the solid and liquid on either side of it, and that a uniform heat generation in the metal film occurs as  $p_{in} = p_o + \epsilon t$ , the temperature of the metal patch modeled as a lumped thermal system is

$$T = T_\infty + \frac{p_o}{S(k_L + k_s)} \left( (1 - e^{-\beta t}) + \frac{\epsilon}{p_o \beta} (\beta t - (1 - e^{-\beta t})) \right) \quad 3$$

where

$$\beta = \frac{S(k_L + k_s)}{v \rho C_p} \quad 4$$

and  $v, \rho_s, C_{ps}, k_L, k_s, T_\infty$  and  $t$  are the metal film volume, density, and specific heat, the liquid and solid thermal conductivities, ambient liquid temperature, and time, respectively. From this simple model, the two cases covered in figure 5 -  $p_{in} = p_o$  for figure 5a (the pulse), and  $p_{in} = \epsilon t$  for figure 5b (the ramp) - are consistent with eq. 3 for both the initial derivatives and curvatures. For long pulse durations ( $t \rightarrow \infty$ ), eq. 3 shows that the square pulse leads to a steady state film temperature while for the ramp input the average surface temperature of the film should increase linearly with time. Though the pulse durations depicted in figure 5 are too short to fully confirm this trend, the results qualitatively suggest them to be consistent with these expectations.

For constant  $V_{in}$  (figure 5a) an inflection point is evident at about 1.7  $\mu s$  into the heating pulse at 265C. The inflection point signifies incipient bubble nucleation. For the ramped power input (figure 5b) a lower nucleation temperature (approximately 205C) at 240 $\mu s$  is found due to the lower heating rate. While these inflection point temperatures show significant superheating of water by over 100C, they are far below the homogeneous nucleation temperature for water [18].

Figure 6 shows the effect of heating rate on inflection point temperature at atmospheric pressure (the heating rate was estimated by linearizing the evolution of temperature from the initial state to the inflection point). Data for both ramp and pulse inputs are shown. The ramp input

facilitated low heating rates (less than  $10^6$  °C/s) while square pulses allowed heating rates up to about  $10^9$  °C /s to be achieved. Between  $10^7$  °C /s and  $10^8$  °C /s the pulse and ramp inputs yielded essentially the same nucleation temperature showing the consistency of the two methods for heating the films.

The nucleation temperature is essentially constant at about 200 °C below a heating rate of about  $10^6$  °C/s and increases at higher rates. This temperature is higher than the 180 °C average temperature measured by Li and Peterson [19] for degassed water on 100  $\mu\text{m}$  square films (AR=1). Nucleation was noted to be initiated in the central portion of the films where a conduction analysis showed the temperature to be 205 °C, thus suggesting significant temperature gradients over the surface. The AR=66.7 platinum film used in the present study for measuring the nucleation temperature should have a negligible temperature distribution along the 100  $\mu\text{m}$  length and provide a more accurate incipient boiling temperature for low heating rates.

Two processes can trigger bubble nucleation: random density fluctuations; and nucleation of pre-existing gas pockets that form by the process of immersing the film in water. For the latter situation, “nucleation” would denote the process of a gas pocket stabilizing at the advancing contact angle and then growing to macroscopic size.

The nucleation temperature of 200 °C is too low for density fluctuations to be a relevant mechanism for a phase transition over the pressure range investigated. On a microscopically smooth surface the bubble shape will be some variant of a truncated sphere depending on the contact angle in the liquid and geometry of the surface. The energy to form a bubble at the surface will be lower than for a spherical bubble but the number density of molecules at the surface ( $N_s$ , molecules/ $\text{m}^2$ ), which may be considered as potential nucleation “sites”, is lower than in the bulk ( $N_o$ , molecules/ $\text{m}^3$ ) with  $N_s : N_o^{2/3}$  [20] so that the probability of homogeneous nucleation at a surface could conceivably be lower than in the bulk for a liquid in contact with a solid. The contact angle for water on most metals is low, generally below about 50° [21] so that the energy barrier for a flat smooth surface is close to the bulk value. As such, homogeneous nucleation in the bulk does not appear to be favored at the low heating rates in figure 6. This leaves the prospect that pre-existing nuclei or gas pockets could trigger bubble nucleation at heating rates below  $10^6$  °C/s.

A mechanism to create gas pockets at surfaces comes from ideas developed by Lorenz et al. [22]. An advancing liquid front on a surface can trap air as the front moves past surface imperfections. Though the microheaters used in the present study are microscopically smooth, they are raised structures with a height of about 230 nm. The corner could serve as a sort of surface

imperfection that traps gas as depicted in figure 2. When the films are immersed in water, liquid floods the surface and spreads over it with an advancing contact angle  $\theta$  as shown in figure 2 (the corners are not as sharp as depicted in figure 2 but have a more rounded shape). Gas pockets could become trapped after full immersion. The effect of bubble nucleation at the corners of intersecting surfaces was also noted in a previous study [23] though in that study density fluctuations were considered as the mechanism for bubble nucleation.

Nucleation of a gas pocket requires achieving a state of static mechanical equilibrium for a critical size bubble that would then begin to grow. For such a bubble,

$$P_{\text{sat}}(T_w) - P_o = \frac{2\sigma(T_w, R_c)}{R_c} \quad 5$$

where it is assumed that  $P_{\text{sat}}(T)$  is the pressure inside a bubble of radius  $R_c$ . The surface tension is related to bubble radius as [24]

$$\sigma = \frac{\sigma_\infty}{1 + \frac{\delta(R_c)}{R_c}} \quad 6$$

where  $\delta$  represents the separation of the equimolar surface from the surface of tension. In the general case it depends on bubble size. A recent study developed numerical predictions for  $\delta$  in terms of radius [25]. From this work and over the range of temperatures of interest in this study, which is between the boiling point of water (373K) and the superheat limit (approximately 573K at atmospheric pressure), the water surface tension is found to be essentially the bulk value,  $\delta/R_c \ll 1$ . At 200 °C (473K),  $\sigma \approx 0.037$  N/m [1] and  $P_{\text{sat}} \approx 1.56$  MPa [26] so that from eq. 5  $R_c \approx 51$  nm for  $P_o = 0.101$  MPa. Given that the thickness of the Pt/Ti layer is 230 nm, it is conceivable that a 51 nm diameter gas pocket could be formed when the platinum films are immersed in water as suggested in figure 2. A critical size bubble of fixed radius would keep the nucleation temperature relatively constant.

With increasing heating rates, density fluctuation processes appear to exert an ever-increasing influence over the nucleation temperature. At the highest rates in figure 6 the homogeneous nucleation temperature for water is approached, even though a gas pocket may already exist at the surface. In this event, bubble nucleation would become a sort of hybrid process influenced by gas pockets and density fluctuations with density fluctuations controlling at the highest heating rates. The matter to consider concerns the relative times to form a bubble of a given size and the time for the surface to reach high temperatures where the probability for homogeneous nucleation is appreciable.

From classical bubble growth theory for heat transfer controlled growth,  $R \sim C_1 t^{1/2}$  [27,28] where  $C_1$  depends on thermal properties ( $C_1 \sim m/s^{1/2}$ ). The time for a bubble to reach a characteristic size  $R = R_{ca}$  (without departing) after it starts growing will therefore scale as

$t_L : \left( \frac{R_{ca}}{C_1} \right)^2$ . For heating at a constant rate ( $\xi$ ) that begins at  $T=T_\infty$  and ends when  $T=T_{nuc}$ ,  $\xi : \frac{T_{nuc} - T_\infty}{t_{nuc}}$ . The liquid will be heated to the nucleation temperature even if gas pockets (pre-

existing bubbles) are present if  $t_{nuc} \ll t_L$  or  $\xi \gg (T_{nuc} - T_\infty) \left( \frac{C_1}{R_{ca}} \right)^2$ . In this case, the liquid is being

heated while a bubble is growing on it but the bubble growth process is too slow to prevent the liquid from being significantly superheated. This is the situation believed to be responsible for the platinum film heaters examined in the present study being capable of approaching the homogeneous nucleation temperature at the highest heating rates while water is in contact with the surface. At

low heating rates,  $\xi \ll (T_{nuc} - T_o) \left( \frac{C_1}{R_{ca}} \right)^2$  and the surface is not heated fast enough before a bubble grows to cover the surface.

Once nucleation occurs, the response of the surface temperature to bubble nucleation and growth is shown in figure 7 for pulse durations of 90  $\mu s$ . The overall form of the variation of temperature qualitatively corresponds to the schematic of figure 1. Interestingly, immediately after the inflection point the temperature is observed to drop slightly, and then quickly recover. This effect may be related to the nucleated bubble rapidly growing over the surface and the vapor temperature momentarily dropping as the bubble absorbs latent heat.

The inflection point temperatures in figure 8 are essentially unchanged as the pressure is reduced. This result would be consistent with homogeneous nucleation theory [18] whereby

$$T_{nuc} \approx C_2 \frac{\sigma^3}{(P_{sat}(T_{nuc}) - P_o)^2}. C_2 \text{ is a constant that depends on, among other variables, the nucleation}$$

rate. Because  $P_{sat}(200 \text{ }^\circ C) \approx 1.48 \text{ MPa}$  and  $P_o < 0.101 \text{ MPa}$ , then  $P_{sat} \gg P_o$  thus making  $T_{nuc}$  virtually independent of  $P_o$  for subatmospheric pressures.

As shown in figure 7, a delay period ensues after nucleation before temperature oscillations begin. This period increases as  $P_o$  decreases. Figure 8, derived from the data in figure 7, further shows this trend. Heat loss from the bubble surface to the ambience is proportional to  $\Delta T = T_{sat}(P_o)$

-  $T_\infty$ . For fixed  $T_\infty$ ,  $\Delta T$  decreases as  $P_o$  decreases (because  $T_{\text{sat}}(P_o)$  decreases with  $P_o$ ) so that heat transfer from the top regions of the bubble surface to the subcooled liquid should decrease (this same argument applies if  $P_o$  is fixed while  $T_\infty$  is increased as discussed below). With reduced heat loss, the bubble can remain at the surface for a longer period and the delay time should then increase. This trend is qualitatively consistent with figures 7 and 8. This same effect should occur if  $P_o$  is fixed (whereby  $T_{\text{sat}}$  is also fixed) and  $T_\infty$  is increased.

Figure 9 shows the evolution of average surface temperature with  $T_\infty$  for  $P_o = 0.101$  MPa and pulse times of 40  $\mu\text{s}$ . As  $T_\infty$  increases the oscillation frequency decreases. This trend is consistent with progressively reduced heat loss from the bubble as  $T_\infty$  is increased for a fixed  $T_{\text{sat}}$  (since  $P_o$  is fixed for the results in figure 9) as noted above. At the highest  $T_\infty$  (93 °C) temperature oscillations completely disappear over the range of the pulse time examined as shown in figure 9. This result suggests a net heat input to the bubble over the duration of the heat pulse, as  $T_{\text{sat}} - T_\infty$  is evidently too low to promote bubble collapse. At  $T_\infty = 93$  °C the surface temperature increases in a manner consistent with the metal film being a lumped thermal system.

The trigger for the onset of temperature oscillations is unknown. A possible mechanism is that the macroscopic bubble or vapor film that covers the surface after nucleation during the waiting period is in a metastable state, balanced by heat input from the film and heat loss to the subcooled liquid. A small perturbation could upset this balance and initiate collapse after which a growth/decay cycle ensues that is manifested by temperature oscillations, assuming that the temperature tracks with the growth/collapse cycle.

The extent to which the surface temperature tracks with the bubble size was determined by simultaneously photographing the surface of the film and recording the surface temperature during a constant heat input. The high speed imaging arrangement used for this purpose requires a fair degree of repeatability of bubble morphology at each instant of the growth/collapse cycle to establish a time sequence of the process from individual images taken at different times in the cycle. We show some results for ethanol boiling on a AR=6.6 film. This smaller AR facilitated confining the bubble volume to the microscope field of view. A 50  $\mu\text{s}$  voltage pulse was imposed on the films.

As shown in figure 10, the bubbles are not spherical during the "growth" and "collapse" phases though they do appear to start out as spherical bubbles (figure 10a, which is close to the inflection point). The critical size bubbles, with predicted radius of about 51 nm (at 200 °C), would be too small to be photographed. The bubbles shown in figure 10 are well into the growth phase and  $P \approx P_o$ . As the bubbles grow, coalescence creates oblong structures (10b, 10c) that loosely conform to the shape of the platinum film footprint. The collapse process (10c-10e) physically breaks up the elongated bubble into smaller bubbles (10e), perhaps by a combination of surface tension and the physical dynamics of the collapse.

The evolution of  $V_{out}$  is shown adjacent to each image in figure 10. Because the AR=6.6 heater was too small to promote a uniform surface temperature, no attempt was made to convert the  $V_{out}$  traces in figure 10 to temperature though we know that  $T_w \propto V_{out}$ . The voltage traces are essentially quasi-static in that repeated pulsing produced almost coincident traces. The red dot indicates the time when the adjacent photograph was taken in the growth/collapse cycle. In the growth phase (10b to 10d) the temperature rises. After collapse where the single large bubble breaks up into smaller structures the surface temperature decreases from 10c to 10e. These trends show that the surface temperature does qualitatively track with the evolution of bubble size (figure 1b and 1c).

We know of no quantitative analysis to predict the trends noted above. Qualitative explanations for surface temperature oscillations during bubble growth and collapse in subcooled liquids [9,12,17,29,30] note the importance of energy loss at the upper regions of the bubble as it grows outside of the superheated liquid layer. During the growth phase the surface temperature increases as the surface is covered with vapor, and there is a net energy input to the bubble. When the bubble penetrates well into the subcooled liquid the bubble begins to lose energy and condensation occurs and the bubble size decreases causing an inflow of cold liquid to the surface that drops the temperature. Repeating this process results in temperature oscillations.

A quantitative explanation of temperature oscillations was obtained by considering a single temperature cycle as schematically shown in figure 1b and 1c. Conditions that would decrease the bubble lifetime  $t_b$  (i.e., the time from growth to collapse) should increase the oscillation frequency. Early bubble growth theories that included predictions of  $t_b$  incorporated an energy loss term to account for condensation of the bubble as it grew beyond the superheated liquid layer adjacent to the surface [30,31].

Few numerical studies related to bubble nucleation and growth at heated surfaces in subcooled liquids considered temperature oscillations during growth/collapse cycles. Wu and Dhir

[32] and Son et al. [33] computed flow patterns around bubbles growing from surfaces into subcooled liquids and showed departure cycles with oscillating Nusselt numbers. Algorithms have also been developed for tracking the detailed shape of bubbles formed in film boiling on superheated surfaces that included the flow dynamics around the growing and departing bubbles [34,35]. Of the many analytical theories that have been developed for bubble growth and collapse, the one by Mikic and Rohsenow [31] offers a relatively simple analytical approach to understanding the trends of the data. This, and similar models [30,36], may be considered to predict the growth/collapse history of a single cycle of an oscillation (figures 1b and 1c). The simplifying assumptions in the model include one-dimensional transport, constant properties, thermally controlled growth, hemispherical bubble, and neglect of surface tension and liquid inertia.

An energy balance on the bubble results in an analytical expression for the evolution of bubble radius as

$$R = \frac{2}{\pi} \sqrt{3} \text{Ja} \sqrt{\pi \alpha t} \left[ 1 - \Theta \left\{ \left( 1 + \frac{1}{(t/t_w)} \right)^{1/2} - \frac{1}{(t/t_w)^{1/2}} \right\} \right] \quad 7$$

where

$$\text{Ja} = \frac{(T_w - T_{\text{sat}}) c_{pL} \rho_L}{h_{fg} \rho_v} \quad 8$$

$$\Theta = \frac{T_w - T_{\infty}}{T_w - T_{\text{sat}}(P_o)} \quad 9$$

and  $t_w$  is the time at which the liquid reaches the nucleation temperature at a distance  $r$  from the surface. There are two roots for  $R=0$  (term in brackets) for eq. 7: one at  $t = 0$  (the initial condition) and another at  $t = t_b$ . Eq. 7 is used to infer how  $\tau \equiv t_b/t_w$  varies with parameters to explain bubble, and hence surface temperature, oscillations. Property values were fixed for all conditions since the theory assumes constant properties. The properties used are listed in Table 1.

Figure 11 shows the predicted variation of  $\tau/\tau_{0.101}$  (i.e., relative to the bubble growth time for  $P_o = 0.101\text{MPa}$ ) with  $P_o$  for the indicated  $T_{\infty}$ . The asymptotes are the saturation pressures corresponding to  $T_{\infty}$  at which state the computed collapse times are infinite (i.e., the bubble does not collapse). The results show that as  $P_o$  decreases the relative bubble growth time increases. Since the surface temperature qualitatively tracks with the growth and collapse cycle (figure 10), an increasing  $\tau/\tau_{0.101}$  implies a decreasing temperature oscillation frequency which is consistent with the data in figures 7 and 8. Similarly, for a fixed  $P_o$  figure 11 also shows that the bubble collapse

time ( $t_b$  or  $\tau/\tau_{0.101}$ ) increases with  $T_\infty$ . By inference, a longer collapse time would correspond to a smaller frequency. This trend is also consistent with figure 9.

## Conclusions

The bubble nucleation temperature is unaffected by pressure in the sub-atmospheric range examined because the internal bubble (vapor) pressure is much greater than the surrounding liquid pressure over the ambient pressure range examined. However, ambient pressure affects the temperature difference driving energy exchange between the bubble and surrounding liquid which in turn influences temperature oscillations. Surface temperature oscillations occur at frequencies that decrease with decreasing subcooling, and increase with increasing pressure. The trends follow qualitative expectations from thermally controlled bubble growth theories that incorporate a heat loss mechanism to the subcooled liquid.

A strong effect of nucleation temperature on heating rate was observed. At low rates ( $<10^6$  °C/s) the nucleation temperature is constant suggesting the presence of gas pockets of a fixed size there are trapped during the liquid spreading process. As heating rate further increases the nucleation temperature approaches the theoretical limit for water at  $10^9$  °C/s, as density fluctuation processes exert an increasing influence on triggering a phase transition even though pre-existing gas pockets may be present. High-speed imaging shows that the evolution of bubble morphology qualitatively tracks with surface temperature in the cyclic temperature history.

## Nomenclature

AR	aspect ratio of heater (length divided by width)
$C_p$	Pt film specific heat ( $\text{J kg}^{-1}\text{K}^{-1}$ )
$g$	acceleration due to gravity ( $\text{m/s}^2$ )
$k_L$	liquid thermal conductivity ( $\text{W}\cdot\text{m}^{-1}\cdot\text{°C}^{-1}$ )
$k_s$	solid thermal conductivity ( $\text{W}\cdot\text{m}^{-1}\cdot\text{°C}^{-1}$ )
L	Length of heater (m)
$N_s$	number density of molecules at the surface (molecules/ $\text{m}^2$ )
$N_o$	number density of molecules in the bulk (molecules/ $\text{m}^2$ )
$p_{in}$	input power (W)
$p_o$	input power (W) for square pulse
$P_o$	ambient pressure
$P_{sat}$	pressure inside the bubble
$R_c$	bubble radius
R	bubble radius
$R_1$	fixed wheatstone bridge resistor ( $\Omega$ )
$R_2$	fixed wheatstone bridge resistor ( $\Omega$ )
$R_3$	adjustable resistor ( $\Omega$ )
$R_H$	heater resistance ( $\Omega$ )
$R_L$	lead resistance due to electrical connections ( $\Omega$ )
$R_T$	$R_L + R_H$ ( $\Omega$ )
$R_\infty$	heater resistance at $T_\infty = 22\text{ °C}$
S	conduction shape factor (m)
t	time (s)
$t_b$	bubble growth time
$t_w$	waiting time
$t_L$	time for a bubble to reach size $R_{ca}$ (s)
T	Platinum temperature ( $\text{°C}$ )
$T_\infty$	ambient fluid temperature ( $\text{°C}$ )
$T_{nuc}$	bubble nucleation temperature ( $\text{°C}$ )
$T_w$	surface temperature ( $\text{°C}$ )

$v$	volume of Pt film
$V_{in}$	input voltage to bridge (V)
$V_o$	voltage amplitude for pulse input (V)
$V_{out}$	bridge output voltage (V)

### Greek

$\alpha$	thermal diffusivity ( $m^2 \cdot s^{-1}$ )
$\delta$	separation of the equimolar surface from the surface of tension (m)
$\theta$	contact angle
$\epsilon$	voltage ramp rate (V/s)
$\rho_L$	density liquid ( $kg \ m^{-3}$ )
$\rho_g$	density gas ( $kg \ m^{-3}$ )
$\rho_s$	density of metal film ( $kg \ m^{-3}$ )
$\sigma$	surface tension
$\tau$	$\equiv t_b/t_w$

### **References**

1. Lienhard, J.H. IV, Lienhard, J.H. V A Heat Transfer Textbook, 3<sup>rd</sup> Edition, pp. 465, 472 Phlogiston Press, Cambridge, MA. (2003)
2. Allen, R.R., Meyer, J.D. Knight, W.R., Thermodynamics and hydrodynamics of thermal ink jets, Hew. Pack. J. 36 (1985) 21-27.
3. Kraemer, T. Printing enters the jet age, Invent. Tech., 16 (2001) 18-27.
4. Staples, M., Daniel, K., Cima, M.J., Langer, R. Application of microand nano electromechanical devices to drug delivery, Pharma. Res. 23 (2006) 847–863.
5. Laser, D.J., Santiago, J.G. A review of micropumps, J. Micromech. Microeng. 14 (2004) R35–R64.

6. Geng, X., Yuan, H., Oguz, H. N., Prosperetti, A., Bubble-based micropump for electrically conducting liquids. *J. Micromech. Microeng.* 11 (2001) 270-276.
7. Chen, T., Klausner, J.F. Chung, J.N. Subcooled boiling heat transfer and dryout on a constant temperature microheater, *Int. J. Heat Fluid Flow* 25(2004) 274-287.
8. Kim, J., Henry, C. Heater Size and Gravity Effects on Pool Boiling Heat Transfer, CP654, Space Technology and Applications International Forum - STAIF 2003, M.S. El-Geng, ed., American Institute of Physics.
9. Avedisian, C. T., Osborne, W. S., McLeod, F. D. and Curley, C. M., Measuring bubble nucleation temperature on the surface of a rapidly heated thermal ink-jet heater immersed in a pool of water. *Proceedings of the Royal Society of London Series a- Mathematical Physical and Engineering Sciences* 455 (1999) 3875-3899.
10. Avedisian, C.T. The thermal ink jet printer: a paradigm for microscale phase change, *Proc. 5<sup>th</sup> ISHMT-ASME Heat and Mass Transfer Conf. and 16<sup>th</sup> National Heat Transfer Conf.* January 3-5 (2002), Calcutta, pp. 169-175, Tata McGraw-Hill (ISBN 0-07-047443-5).
11. S.A. Zhukov, V.A. Rafeev, S. Yu, S.B. Afans'ev, S.B. Echmaev, B.L. Korsunksii, Singularities of realization of film boiling on wire heaters. *High Temperature* 41 (2003) 243-251.
12. Romera-Guereca, G., Choi, T. Y., Poulidakos, D., Explosive vaporization and microbubble oscillations on submicron width thin film strip heaters. *International Journal of Heat and Mass Transfer* 51 (2008) 4427-4438.
13. Avedisian, C. T., Cavicchi, R. E., Tarlov, M. J., New technique for visualizing microboiling phenomena and its application to water pulse heated by a thin metal film. *Review of Scientific Instruments* 77 (2006) 063706.
14. Thomas, O. C.; Cavicchi, R. E.; Tarlov, M. J., Effect of surface Wettability on fast transient microboiling behavior. *Langmuir* 19 (2003) 6168-6177.

15. Cavicchi, R.E., Avedisian, C.T. Bubble Nucleation and Growth Anomaly for a Hydrophilic Microheater Attributed to Metastable Nanobubbles, *Physical Review Letters*, 98 (2007) 124501.
16. Balss, K.M., Avedisian, C.T., Cavicchi, R.E., Tarlov, M.J. Imaging Microboiling Behavior on Pulsed Heated Au Films Modified with Hydrophilic and Hydrophobic Self-Assembled Monolayers, *Langmuir* 21(2005) 10459-10467.
17. Lee, H.S., Merte, H. The Origin of the Dynamic Growth of Vapor Bubbles Related to Vapor Explosions, *J. Heat Transf.* 120 (1998) 174-182.
18. Avedisian, C.T., The Homogeneous Nucleation Limits of Liquids, *J. Phys. Chem. Ref. Data*, 14 (1985) 695-720.
19. Li, J., Peterson, G. P., Boiling nucleation and two-phase flow patterns in forced liquid flow in microchannels. *International Journal of Heat and Mass Transfer* 48 (2005) 4797-4810.
20. Apfel, R.F. Vapor cavity formation in liquids, Technical Memorandum #62, Acoustics Research Laboratory, Harvard Univ., Cambridge (1970).
21. Adamson, A. W., Gast, A. P. *Physical chemistry of surfaces*, 6th edn, (1997) pp. 365-366. Wiley.
22. Lorenz, J.J., Mikic, B.B., Rohsenow, W.M. The effect of surface conditions on boiling characteristics, Report No. DSR 73413-79, Department of Mechanical Engineering, Engineering Projects Laboratory, Massachusetts Institute of Technology, Cambridge, December 1972 (also Proc. 5<sup>th</sup> Int. Heat Transf. Conf. Vol. 5 (1974), Hemisphere, New York).
23. Li, J. Cheng, P. Bubble cavitation in a microchannel, *Int. J. Heat Mass Trans.* 47 (2004), 2689-2698.
24. Tolman, R.C. The effect of drop size on surface tension, *J. Chem. Phys.* 17 (1949), 333-337.

25. Bartell, L.S. Tolman's  $\delta$ , surface curvature, compressibility effects and the free energy of drops, *J. Phys. Chem. B* 105 (2001), 11615-11618.
26. Incropera, F.P., DeWitt, D.P. "Introduction to Heat Transfer," 4<sup>th</sup> Edition (2002) 838,839.
27. Avedisian, C.T. Bubble Growth in Superheated Liquid Droplets, *Encyclopedia of Fluid Mechanics*, Chapter 8 (1986), pp. 130-190, Gulf Publ. Co. Houston.
28. Prosperetti, A., Plesset, M. Vapour-bubble Growth in a Superheated Liquid, *J. Fluid Mechanics*, 85 (1978) 349-368.
29. Moore, F.D., Mesler, R.B. The measurement of rapid surface temperature fluctuations during nucleate boiling of water, *AIChEJ.* 7 (1961) 620-624.
30. Zuber, N. The dynamics of vapor bubbles in nonuniform temperature fields, *Int. J. Heat Mass Transf.* 2 (1961) 83-98.
31. Mikic, B.B., Rohsenow, W.M. Bubble Growth Rates in Non-Uniform Temperature Field, *Prog. Heat Mass Transf.* 2 (1969), pp. 284-292.
32. Wu, J., Dhir, V.K. Numerical simulations of the dynamics and heat transfer associated with a single bubble in subcooled pool boiling, *J. Heat Transfer* 132 (2010), 111501.
33. Son, G., Dhir, V.K., Ramanujapu, N. Dynamics and Heat Transfer Associated With a Single Bubble During Nucleate Boiling on a Horizontal Surface, *J. Heat Transfer* 121 (1999) 623-631.
34. Esmaeeli, A., Tryggvason, G. Computations of film boiling. Part I: numerical method *Int. J. Heat Mass Transf.* 47 (2004) 5451-5461.
35. Banerjee, D., Dhir, V.K. Study of Subcooled Film Boiling on a Horizontal Disc: Part 2—Experiments, *J. Heat Transf.* 123 (2001) 285-293.

36. Nishikawa, K., Kusuda, H., Yamasaki, K. Growth and collapse of bubbles in nucleate boiling, Bulletin of the JSME 8 (1965) 205-210.

Table 1: Water property values (evaluated at 403K)

$\sigma$ (N/m)	$\rho_L$ (kg/m <sup>3</sup> )	$\rho_v$ (kg/m <sup>3</sup> )	$C_{pL}$ (J/kg-K)	$C_{pv}$ (J/kg-K)	$h_{fg}$ (J/kg)	$k_L$ (W/m-K)	$\mu_L$ (kg/s-m)
0.053	934.	1.51	4266.	2177.	$2.17 \times 10^6$	0.688	$2.10 \times 10^{-3}$

## Figure Captions

Figure 1: a) Illustration of temperature history for a pulse-heated microheater showing the stages prior to temperature oscillations. b) Representation of one cycle of a temperature oscillation. c) Suggested correspondence of one bubble growth and collapse cycle with a temperature cycle.

Figure 2: Cross section of the thin film structures (not to scale). Also shown is a potential mechanism for trapping a gas pocket in the corner of the raised metal film as the liquid with advancing contact angle  $\theta$  spreads over the surface.

Figure 3: Photomicrograph (top view) of an AR=66.7 platinum heater. Light area Pt and dark area is Si.

Figure 4: Schematic of bridge circuit. The dotted box is a pressure chamber.

Figure 5: Influence of input waveform on average film temperature: a) pulse input,  $V_{in}=12.9$  V; b) ramp input.  $V_{out}$  is converted to temperature which is along the left axis while the right axis shows the form of  $V_{in}$ . Arrows on the curves indicate which axis corresponds to the data of that curve.

Figure 6: Nucleation temperature as a function of heating rate. The heating rate was approximated as in figure 5.

Figure 7: Effect of ambient pressure on the evolution of surface temperatures for 90  $\mu$ s pulse widths showing features that roughly correspond to figure 1. Pressure is given in the inset to the figures. Applied pulse voltage was 6.6 V. Device aspect ratio AR=10.

Figure 8: Variation of frequency (filled squares) and delay time (filled circles) for the first oscillation cycle with ambient pressure.

Figure 9: Evolution of surface temperature,  $t$  for 40  $\mu$ s pulse widths at various ambient temperatures,  $T_{\infty}$  for  $P_o = 0.101$ MPa.

Figure 10: Photographs of bubbles at various stages of one cycle of a growth and collapse sequence. The fluid is ethanol and the pulse duration is 30  $\mu$ s. The photographs and  $V_{out}$  measurements were taken simultaneously. The "dots" placed on the voltage traces adjacent to each photograph correspond to the time of the laser flash that provided the illumination for the photograph. The total range of the voltage plot is 0.35 V for all six traces. The device was 7  $\mu$ m x 46  $\mu$ m with an aspect ratio AR=6.6 .

Figure 11: Variation of computed nondimensional bubble growth/collapse time (from eq. 7),  $\tau=t_b/t_w$ , normalized by the nondimensional time  $(\tau_{0.101})$   $P_o = 0.101$ MPa. The parameter is the bulk liquid temperature,  $T_{\infty}$ . Dotted lines are asymptotes indicate the saturation pressure corresponding to  $T_{\infty}$  at which the normalized growth/collapse time is infinite.

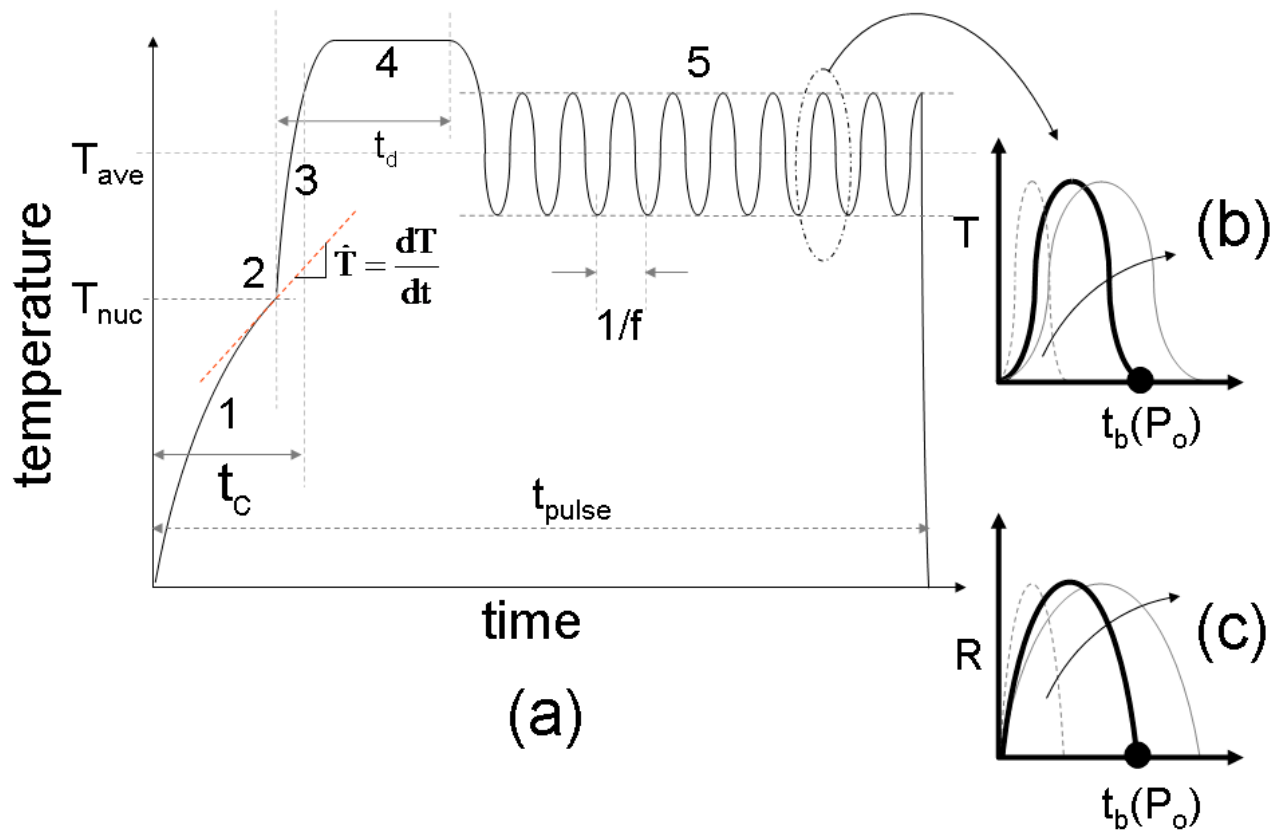


Figure 1

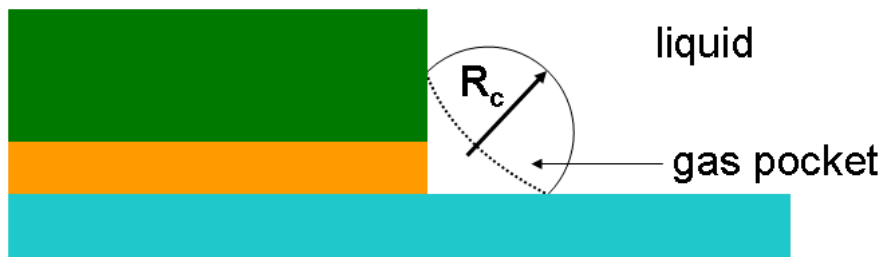
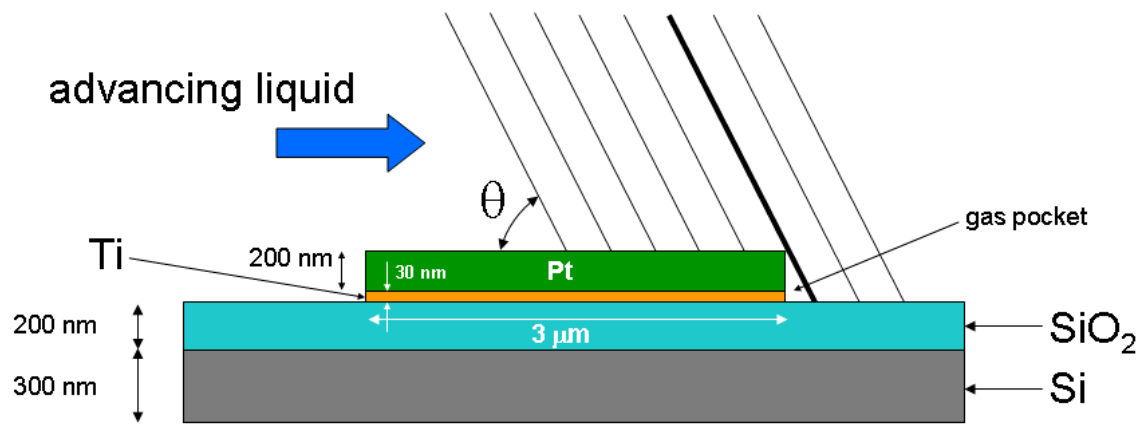


Figure 2

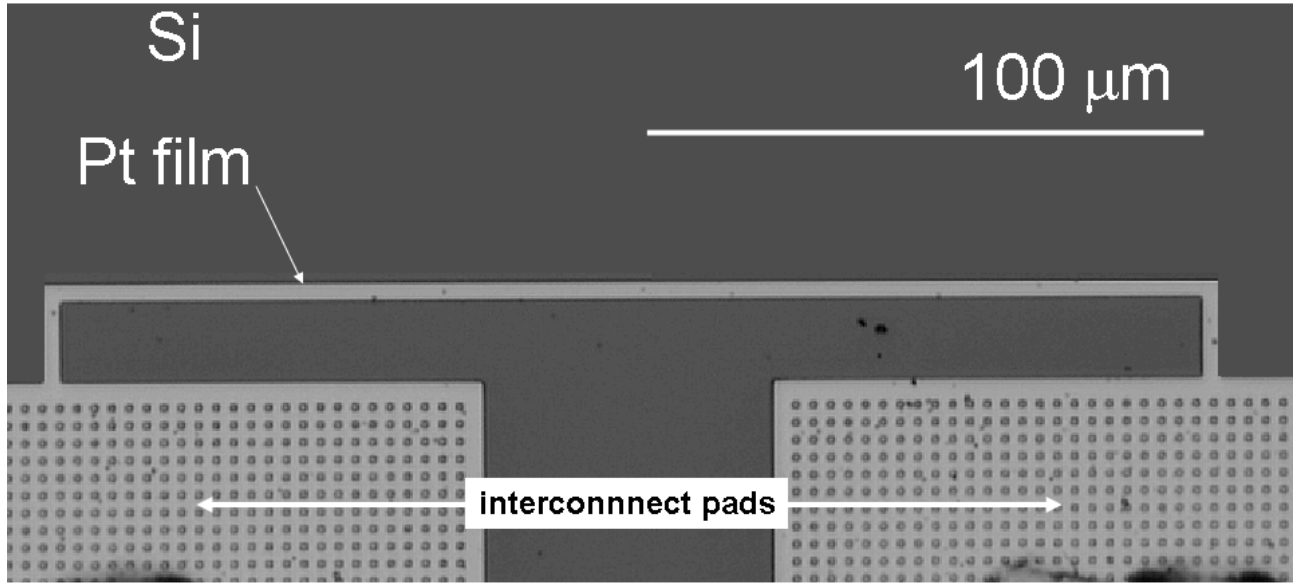


Figure 3

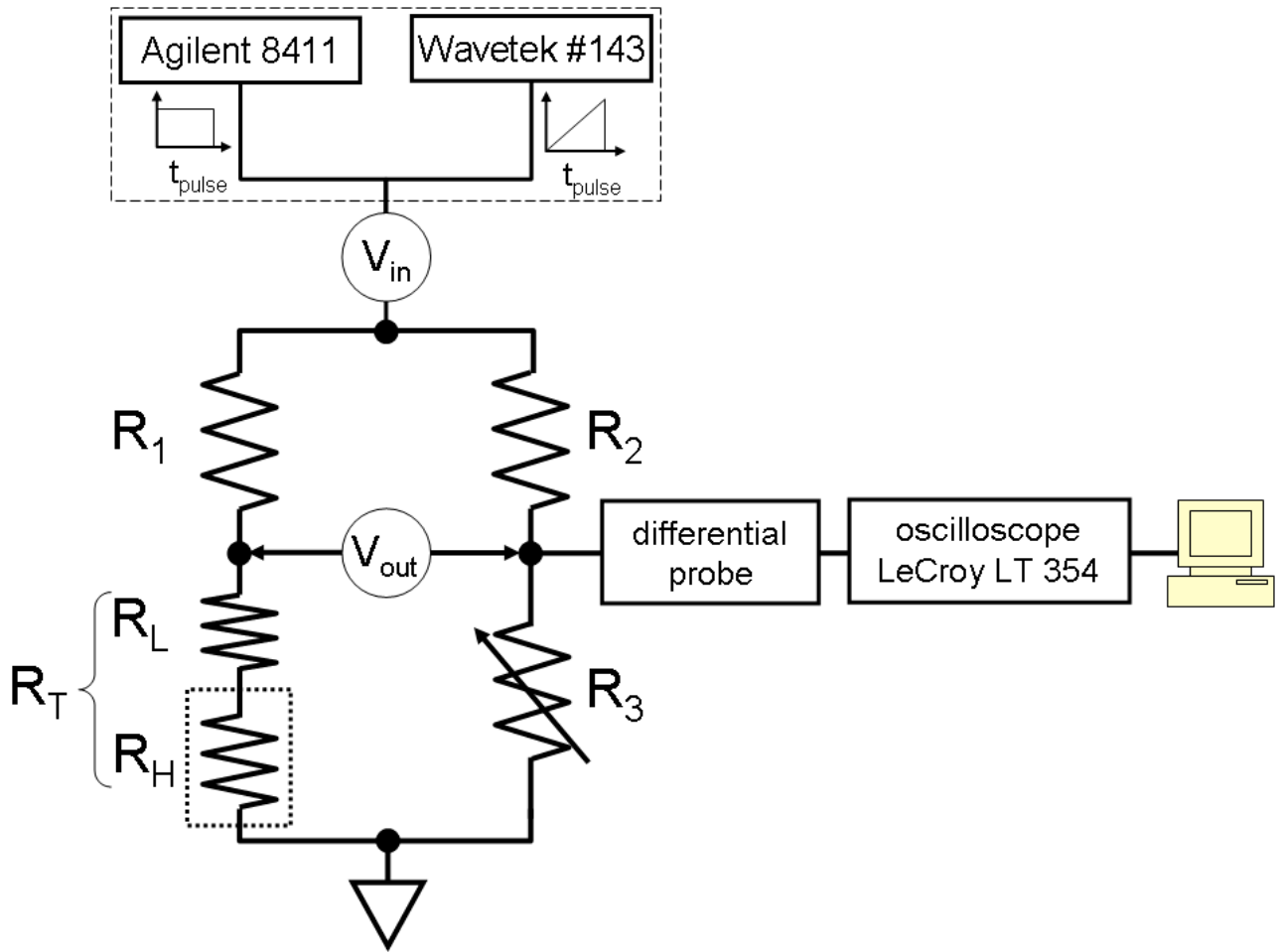


Figure 4

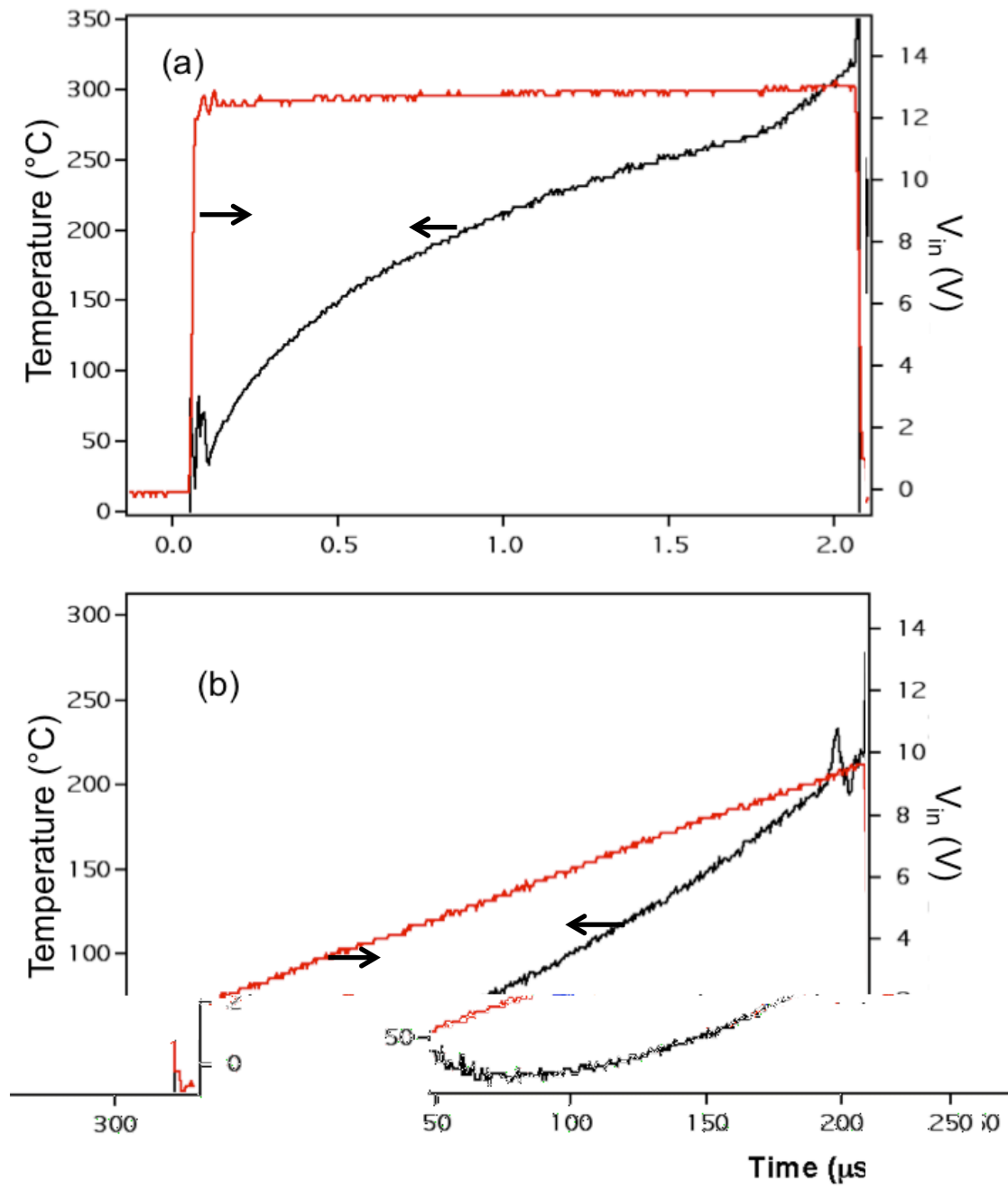


Figure 5

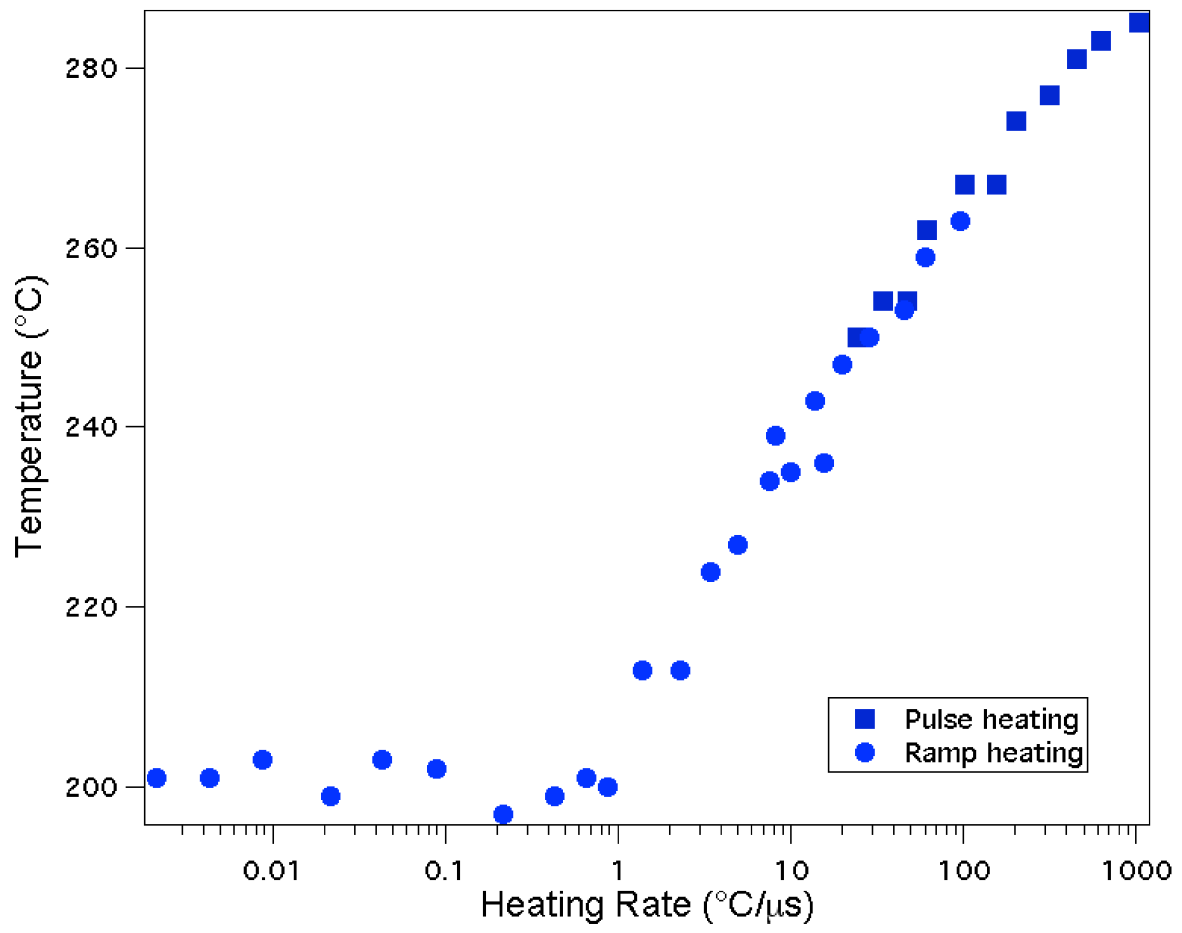


Figure 6

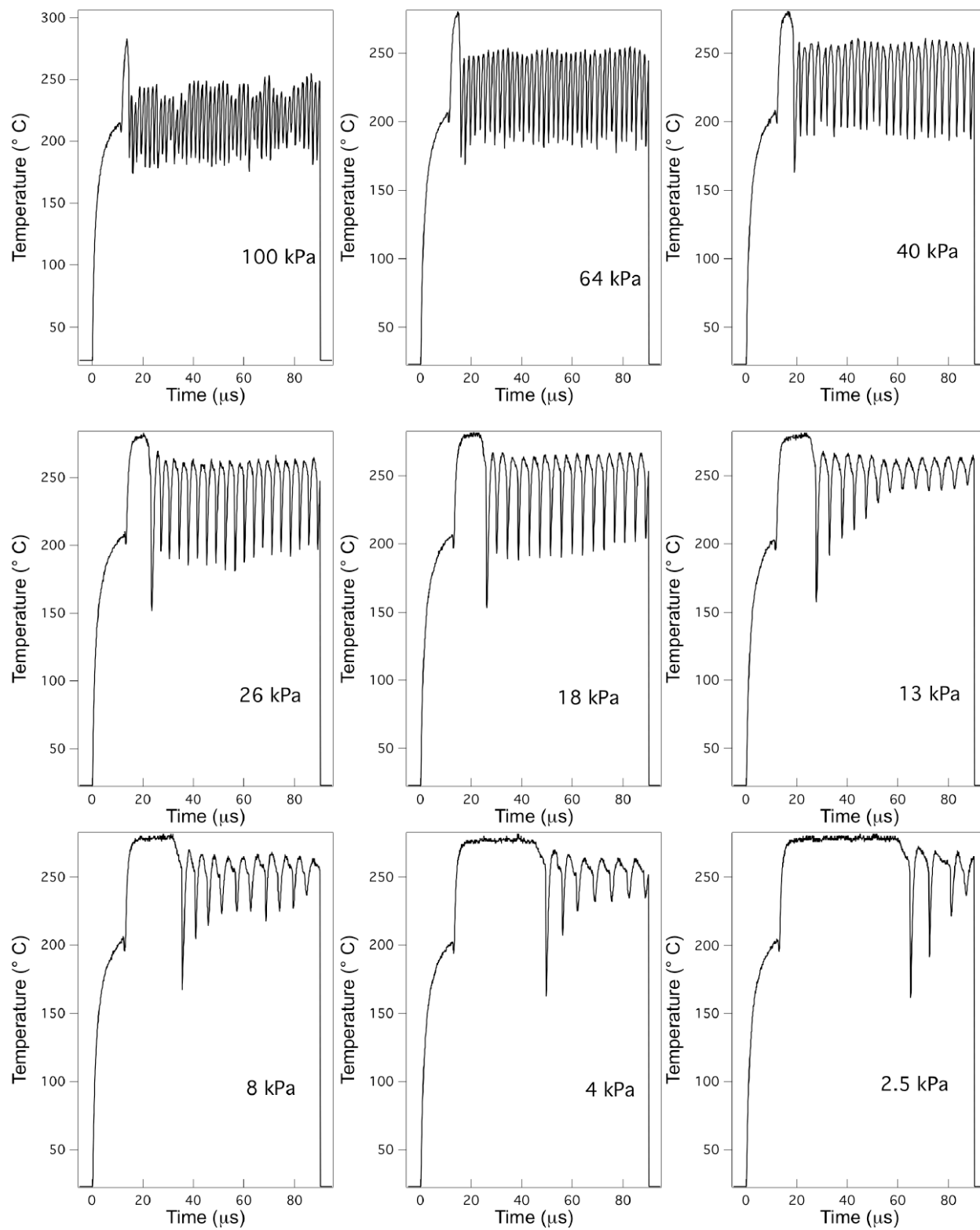


Figure 7

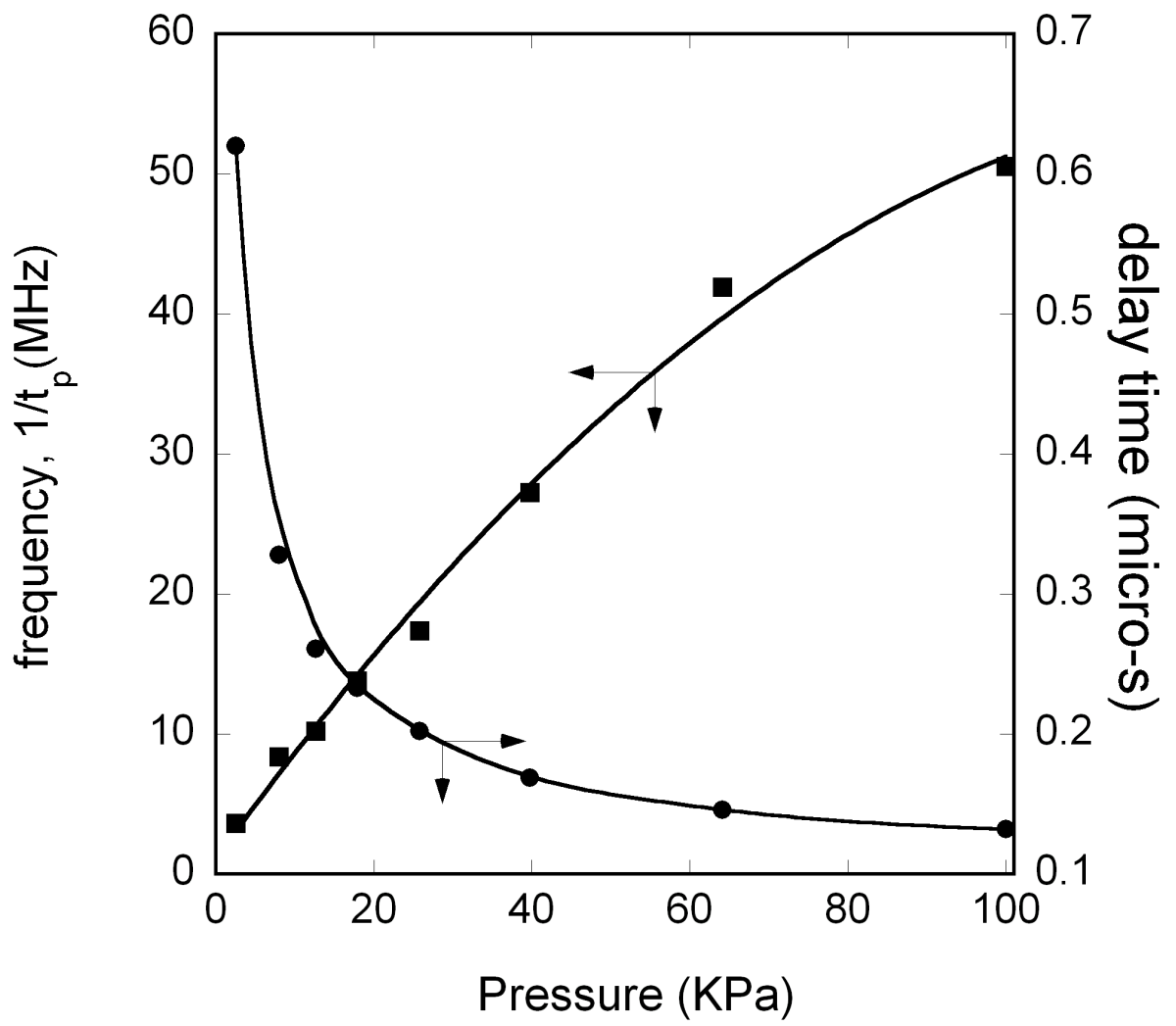


Figure 8

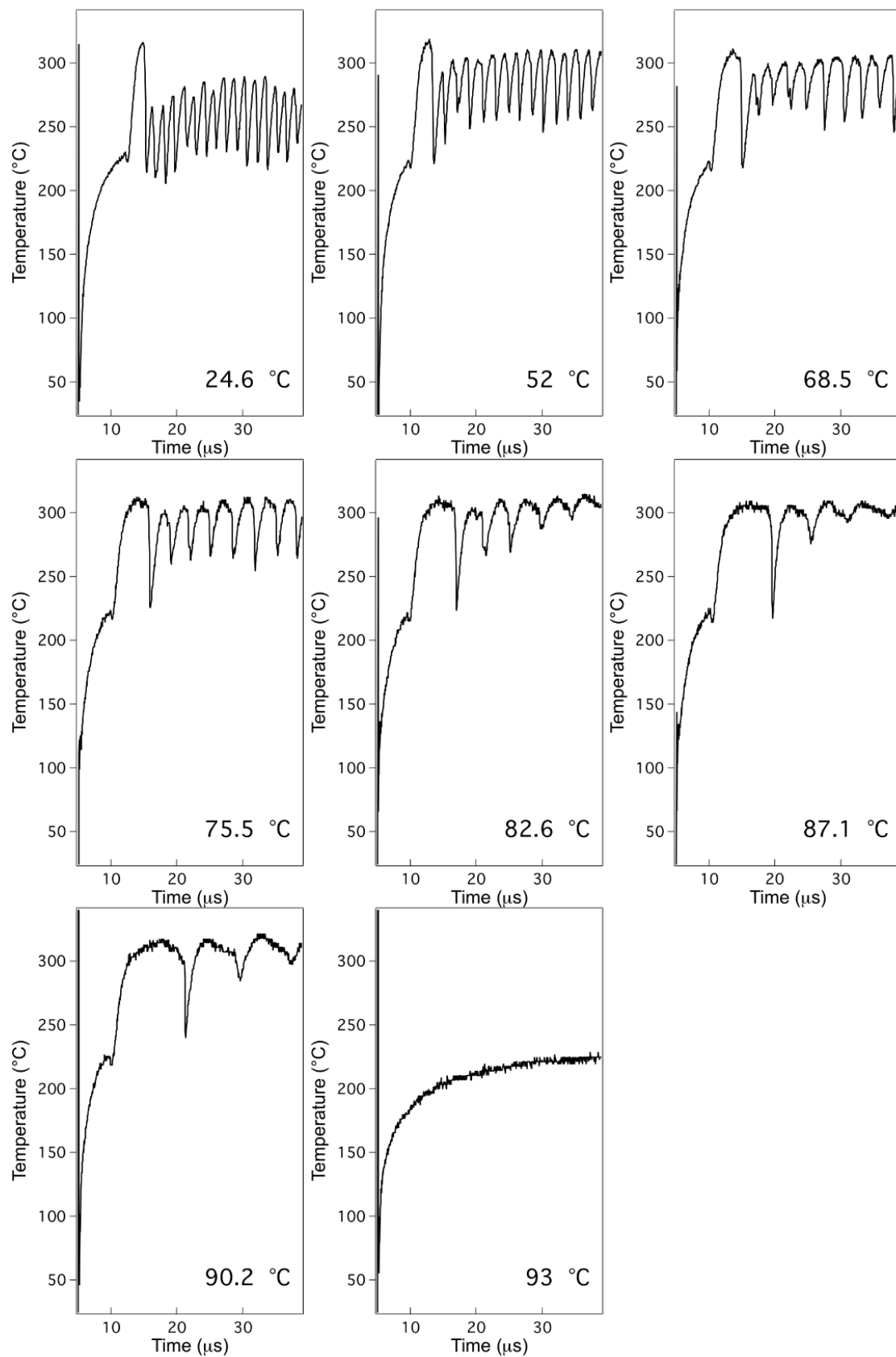


Figure 9

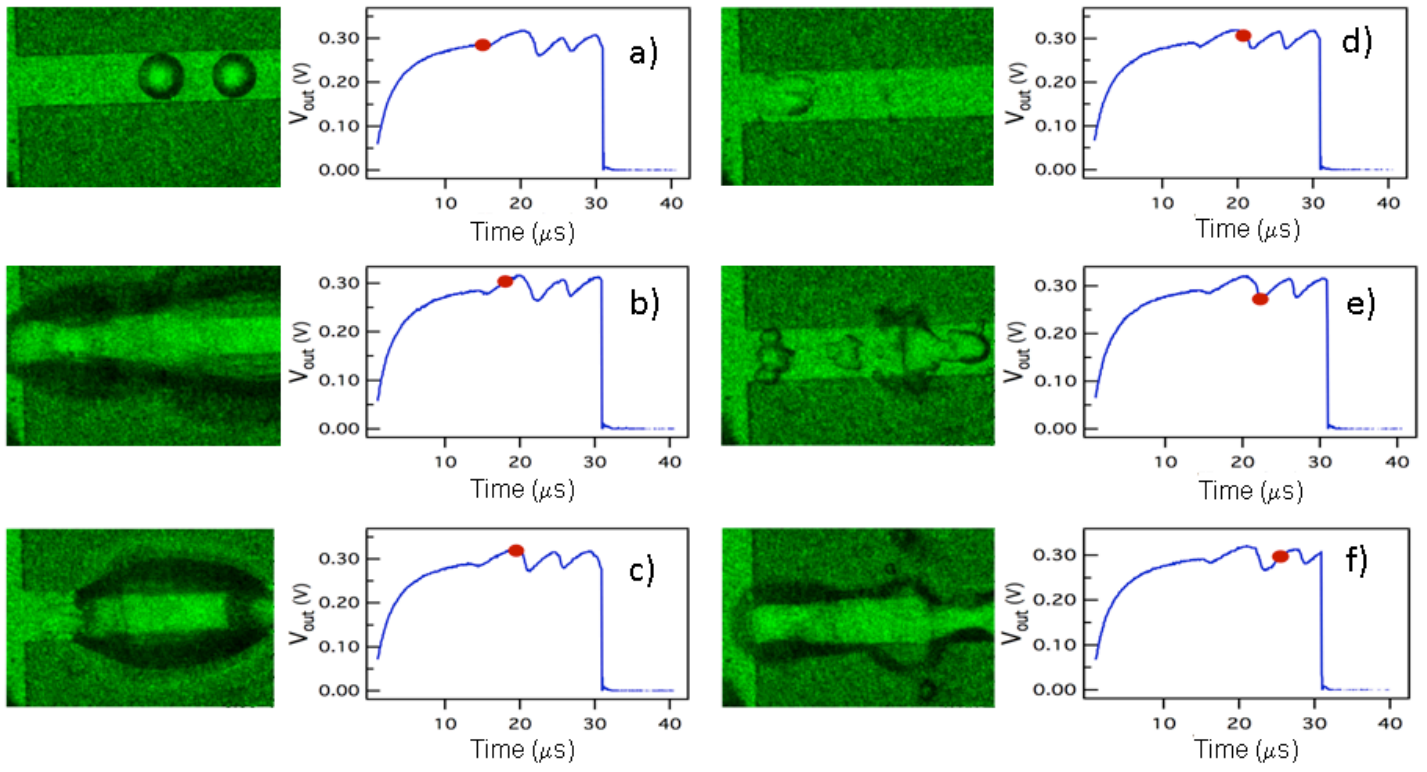


Figure 10

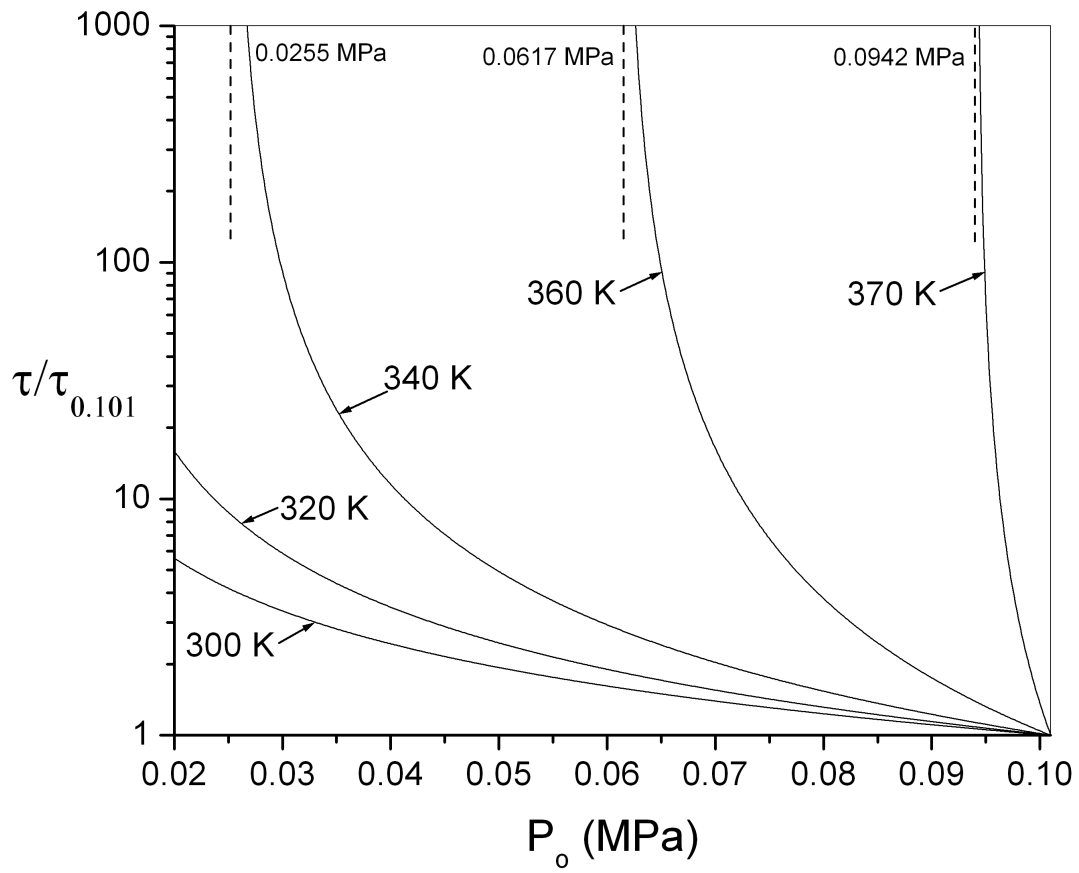


Figure 11